

## Preparation and Optical Characterization of Mesoporous Silica Films with Different Pore Sizes

Jae Young Bae,\* Suk-Ho Choi,<sup>†</sup> and Byeong-Soo Bae<sup>‡</sup>

*Department of Chemistry, College of Natural Science, Keimyung University, Daegu 704-701, Korea. \*E-mail: jybae@knu.ac.kr*

*<sup>†</sup>College of Electronics and Information and Institute of Natural Sciences, Kyung Hee University, Suwon 449-701, Korea*

*<sup>‡</sup>Department of Materials Science and Engineering, Korea Advanced Institute of Science and Technology (KAIST),*

*Daejeon 305-701, Korea*

*Received June 15, 2006*

Mesoporous silica films with three different pore sizes were prepared by using cationic surfactant, non-ionic surfactant, or triblock copolymer as structure directing agents with tetramethylorthosilicate as silica source in order to control the pore size and wall thickness. They were synthesized by an evaporation-induced self-assembly process and spin-coated on Si wafer. Mesoporous silica films with three different pore sizes of 2.9, 4.6, and 6.6 nm and wall thickness ranging from ~1 to ~3 nm were prepared by using three different surfactants. These materials were optically transparent mesoporous silica films and crack free when thickness was less than 1  $\mu\text{m}$ . The photoluminescence spectra found in the visible range were peaked at higher energy for smaller pore and thinner wall sized materials, consistent with the quantum confinement effect within the nano-sized walls of the silica pores.

**Key Words :** Mesoporous silica films, Block copolymers, Photoluminescence, Quantum confinement effect

### Introduction

Scientists at Mobil Corporation synthesized silica-based mesoporous molecular sieves with hexagonal, cubic, and lamellar structure called M41S materials in 1992.<sup>1</sup> For possible applications of mesoporous materials as sensors and optical materials, it is important to develop thin film materials. Zhao, Yang, and Stucky<sup>2</sup> reported dispersion of a bulk silica phase into a liquid which was dip-coated onto silicon wafers and glass slide that resulted in a continuous, uniform coating of colloidal particles. Ogawa<sup>3</sup> described a rapid synthesis route for films in which a mixture of tetramethylorthosilicate was hydrolyzed under acid conditions with substoichiometric amounts of water and cetyltrimethylammonium chloride and then spin coated on glass substrates. The highest application promise is the use of mesoporous silica films as low dielectric constant ( $k$ ) materials<sup>4</sup> with  $k$  preferable lower than 2. Mesoporous silica films are promising for applications such as sensors, optical devices, optical amplifiers, and electrochromic displays.<sup>5</sup>

Recently, visible photoluminescence (PL) from silica-based mesoporous materials has received strong attention due to its potential optoelectronic device applications.<sup>6-8</sup> In order to obtain expectable and controllable light from these materials, it is very important to understand their light-emission mechanism. Two physical models involving excitonic recombination have been proposed to explain the light-emitting properties of the mesoporous silica-based materials.<sup>6</sup> The first model is based on the quantum confinement effect widely used in nanostructured semiconductors and the second one takes into account laser heating due to the collisions of free excitons under intense laser exposure. In contrast, the PL bands in the red and near-infrared spectral

range have been explained in terms of the formation of combined defects involving nonbridging oxygen in silica.<sup>7,8</sup>

In this study, mesoporous silica films with three different pore sizes have been synthesized by rapid solvent evaporation during a spin coating process using tetramethylorthosilicate (TMOS) and alkyl-ammonium halide cationic surfactant (CTACl), polyoxyethylene cetyl ether non-ionic surfactant (Brij 56), or poly(ethylene oxide)-poly(propylene oxide)-poly(ethylene oxide) (PEO-PPO-PEO) triblock copolymer (F 68) as a silica source and a template, respectively. The structural and optical properties of mesoporous silica films with three different pore sizes are investigated using FT-IR, XRD, TGA, TEM, SEM, AFM, UV/VIS/NIR spectrophotometer, and PL spectrometer.

### Experimental Section

**Preparation of mesoporous silica films with three different pore sizes.** Mesoporous silica films with three different pore sizes were prepared following the literature procedure.<sup>9-11</sup> The following chemicals were used without further purification: tetramethylorthosilicate (TMOS, Aldrich, 98%) was hydrolyzed under acidic conditions (HCl, J.T. Baker, 36.5-38%), and then methanol (MeOH, Merck, 99.8%) was added into the hydrolyzed TMOS at room temperature. Finally, CTACl ( $\text{CH}_3(\text{CH}_2)_{15}\text{N}^+(\text{CH}_3)_3\text{Cl}^-$ , Aldrich, 25 wt %), Brij 56 ( $\text{C}_{16}\text{H}_{33}(\text{OCH}_2\text{CH}_2)_{10}\text{OH}$ , Aldrich, 4 wt %), or Pluronic F 68 ( $\text{OH}(\text{CH}_2\text{CH}_2\text{O})_{77}(\text{CHCH}_3\text{CH}_2\text{O})_{29}(\text{CH}_2\text{CH}_2\text{O})_{77}\text{H}$ , Sigma, 10 wt %) as structure directing agents were added so that the final reactant mole ratios were 1-3 TMOS : 8-16  $\text{H}_2\text{O}$  : 0.09-0.11 HCl : 18-30 MeOH : 0.2-0.8 surfactant. The mixture was allowed to react for further 24 hours at room temperature to achieve oligomerization.

The prepared solution was then deposited on Si wafers using the spin-coating method. The silica-surfactant composite thin films were pre-dried at 60 °C, 130 °C and 200 °C for 1 hour at each stage under increasing heat procedure to remove the solvent, water, and organic template. The pre-dried films were calcined in flowing air at 450 °C for 12 hours at the rate of 1 °C/min to remove the organic template thoroughly.

**Characterization of mesoporous silica films with three different pore sizes.** The transparent silica films were characterized using various methods as follows. Infrared spectroscopy was measured by a Bruker EQUINOX55 FT-IR. X-ray diffraction (XRD) patterns of all mesoporous silica films were obtained on a Rigaku D/MAX-RC diffractometer with Cu K $\alpha$  radiation (40 kV, 80 mA) at 0.01° step width and 1 second step time over the range  $1.2^\circ < 2\theta < 10^\circ$ . Thermogravimetric analysis (TGA) of the silica films was performed on a TGA 2050 analyzer from TA Instruments with a heating rate of 10 °C min<sup>-1</sup> in nitrogen. Transmission electron micrographs (TEM) of the calcined silica films were recorded on a JEOL JEM-2000EX electron microscope operating at 200 kV. Scanning electron microscopy (SEM) images were recorded on a Philips 535 M apparatus operating at 20 kV. The surface roughness of the silica films was measured by an atomic force microscopy (AFM) with an Autoprobe 5 M from Park Scientific Instruments. The light transmission spectra were recorded using a Shimadzu UV-3010PC spectrophotometer.

**Photoluminescence of mesoporous silica films with three different pore sizes.** Photoluminescence (PL) spectra were measured using the 488 nm line of an Ar ion laser as the excitation source. For PL measurements, the specimen was mounted on the cold finger in the vacuum chamber (pressure < 10<sup>-5</sup> torr) of a closed-cycle refrigerator. The emitted light was collected by a lens and analyzed using a single monochromator with 1 m focal length and a GaAs cathode photomultiplier. Standard lock-in detection techniques were used to maximize the signal-to-noise ratio. The incident laser beam diameter was about 0.3 mm and the power was about 20 mW.

## Results and Discussion

**Mesoporous silica films with three different pore sizes.** The as-synthesized mesostructured silica films with three different pore sizes were expected to have both solvent and surfactants. The weight loss at about 60 °C, 260-350 °C indicates the desorption of solvent and the decomposition of surfactants, respectively. Figure 1 shows the FT-IR spectra of the as-synthesized and cumulatively heated samples at various temperatures. The two bands appearing at about 2856 cm<sup>-1</sup> and 2926 cm<sup>-1</sup> were due to the C-H stretching vibration modes coming from the surfactant in Figure 1(a). The decreasing intensity of the two bands associated with C-H stretching vibrations with increasing heat treatment temperature suggests the gradual removal of the surfactant from the as-synthesized films. In Figure 1(b), the other

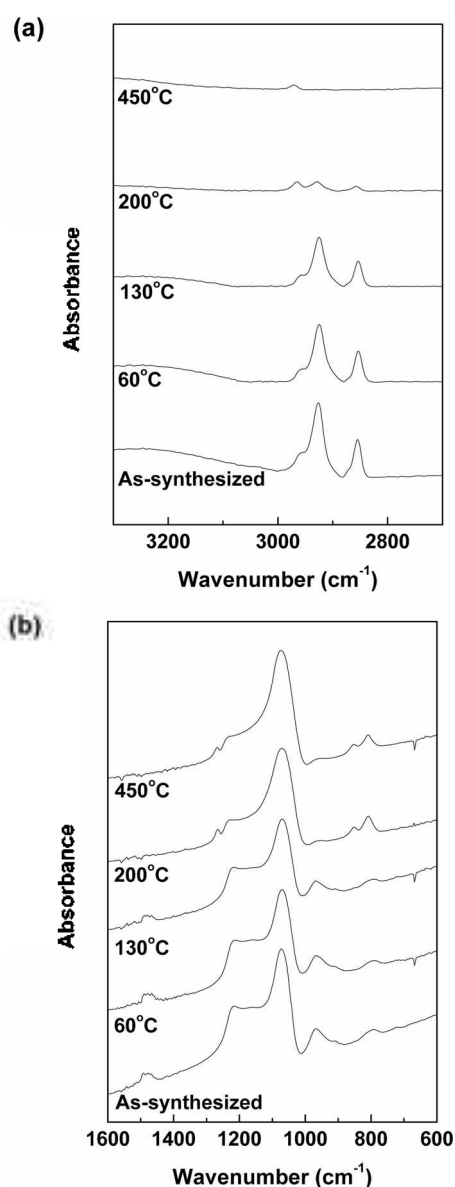


**Figure 1.** FT-IR spectra of (a) C-H stretching vibration modes of surfactant and (b) silica, silanol, and methoxy modes of silica network in the mesoporous silica films annealed at various temperatures.

bands appearing at around 1072 and 791 cm<sup>-1</sup> were associated with Si-O-Si asymmetric and symmetric bond stretching, respectively. The band at around 970 cm<sup>-1</sup> was assigned to the Si-OH, whereas the same band appeared at 960 cm<sup>-1</sup> in the case of the bulk alkoxide-derived silica gel.<sup>12</sup> The absence of C-H stretching vibration modes and silanol group for samples heated at 200 °C indicated the reconstruction of the interfaces, *i.e.*, the complete removal of the surfactant via the decomposition and dehydration of Si-OH groups. The condensation of the silanol groups was expected during the thermal treatment of the gel film.

XRD patterns of as-synthesized and calcined mesoporous silica films with three different pore sizes in Figure 2 indicate that a mesoporous structure was formed on Si wafer. XRD patterns showed a prominent peak at  $2\theta = 1.0\text{--}4.0^\circ$  and

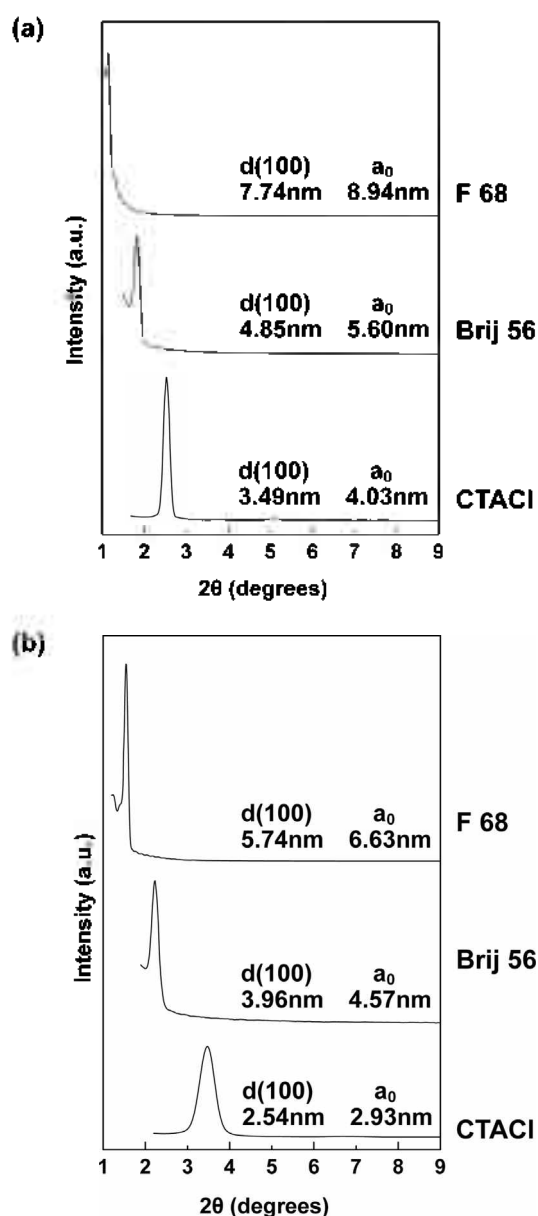


**Figure 2.** XRD patterns of (a) as-synthesized and (b) calcined mesoporous silica films with different pore sizes using various surfactant templates.

some broad peaks at  $2\theta = 4.0\text{--}7.0^\circ$ , which were characteristic of the mesostructure. The unit cell parameter<sup>13</sup> ( $a_0$ ) for the mesostructure is calculated from  $d(100)$  according to  $(a_0) = 2d(100)/3^{1/2}$  where  $d(100)$  is obtained from the  $2\theta$  value of the first peak in the XRD pattern from  $d(100) = \lambda/2\sin\theta$  where  $\lambda = 0.15417$  nm for the Cu  $K\alpha$  line. The unit cell parameter  $a_0$  is equal to the internal pore diameter plus one pore wall thickness. As-synthesized mesostructured silica films with three different pore sizes were prepared by using CTACI, Brij 56, or F 68 and Figure 2(a) shows  $d(100)$  value of 3.49, 4.85, or 7.74 nm and the unit cell parameter of 4.03, 5.60, or 8.94 nm, respectively. According to the XRD patterns, the mesostructure is retained even after decomposition of surfactant by calcination at  $450^\circ\text{C}$  in flowing air for 12 hours. The XRD of calcined mesoporous silica films with three different pore sizes as shown in Figure 2(b) is similar to that prior to calcination except for a substantial decrease in  $d(100)$  value of 2.54, 3.96, or 5.74 nm and the unit cell parameter of 2.93, 4.57, and 6.63 nm, respectively. The broadening of the main peak on calcination suggests less structural ordering in the film after calcination.<sup>14-16</sup>

The ordered structures of the calcined hexagonal mesoporous silica films with three different pore sizes using various surfactant templates were further confirmed by cross-sectional TEM images, as shown in Figure 3. In TEM results, when CTACI, Brij 56, or F 68 was used as template, the inner pore size of mesoporous silica film is about from  $\sim 2$  to  $\sim 3.5$  nm and wall thickness ranging from  $\sim 1 \pm 0.1$  to  $\sim 3 \pm 0.2$  nm, respectively. According to XRD and TEM results, we have known that the thickness of silica walls increases as the pore size of mesoporous silica films increases.

Mesoporous silica film thickness is 200-700 nm as measured by cross-sectional SEM, as shown in Figure 4(a). Mesoporous silica film thickness depends on initial surfactant or methanol concentration. The surface roughness of mesoporous silica film was studied by AFM, and the average roughness is estimated to be less than 1 nm over a length span of  $10\ \mu\text{m}$ , as shown in Figure 4(b). Figure 5 shows the optical transmission spectra of quartz slides coated with mesoporous silica films and the optical transmission of these films is over 92% in visible range. These films have optically transparent mesoporous silica films and no cracks when thickness is less than  $1\ \mu\text{m}$ .

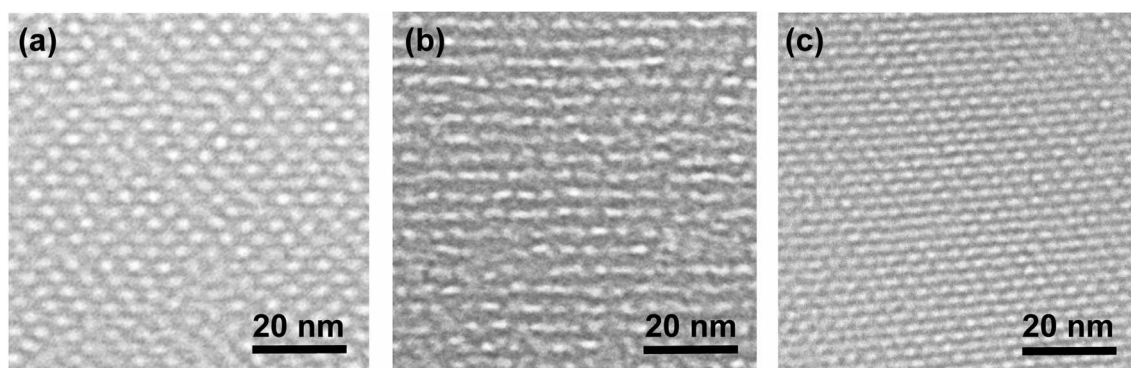


**Figure 3.** Cross-sectional TEM images of mesoporous silica films with different pore sizes using (a) F 68, (b) Brij 56, and (c) CTACI.

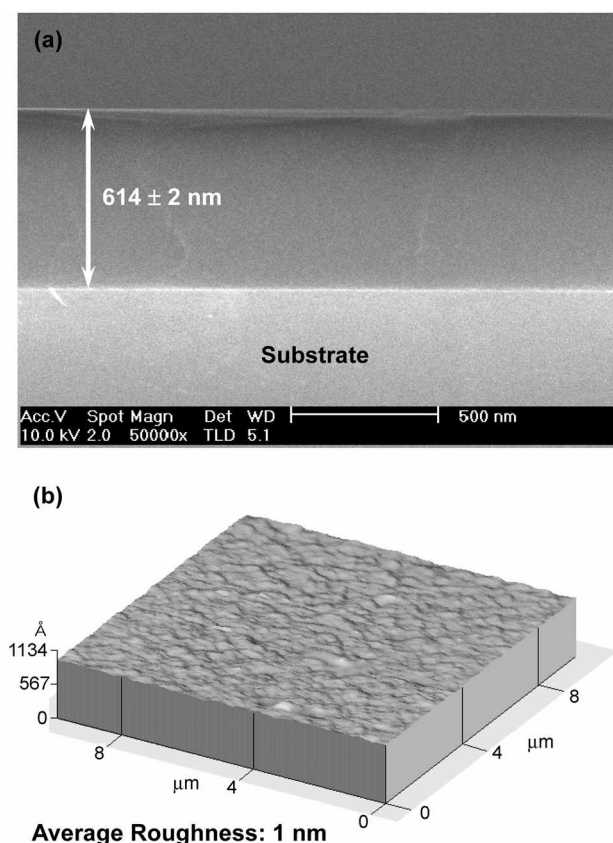


**Figure 4.** (a) Cross-sectional SEM image and (b) top-view AFM image of calcined mesoporous silica films. The surface roughness of mesoporous silica film is around 1 nm.

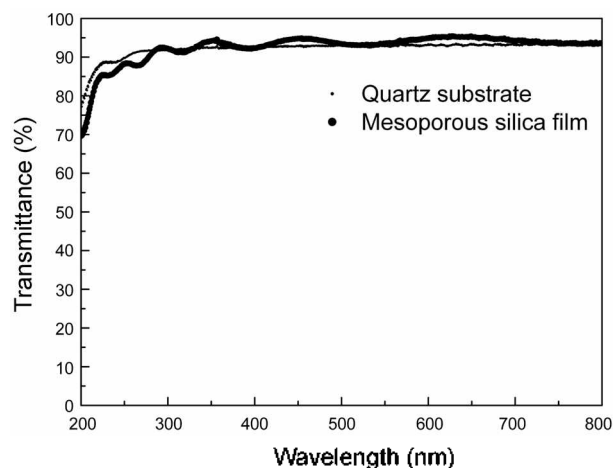


**Figure 5.** Light transmission of quartz slides coated with mesoporous silica films.

**PL of mesoporous silica films with three different pore sizes.** Figure 6 shows PL spectra of mesoporous silica films with different pore size and wall thickness at 8 K. Almost no PL spectra were observed for pure  $\text{SiO}_2$  films without mesopores. No PL was also found in the mesoporous silica films prepared using surfactant templates Brij 56, which is similar to PL spectrum of pure  $\text{SiO}_2$  without mesopores. This result is caused by less mesostructural ordering and

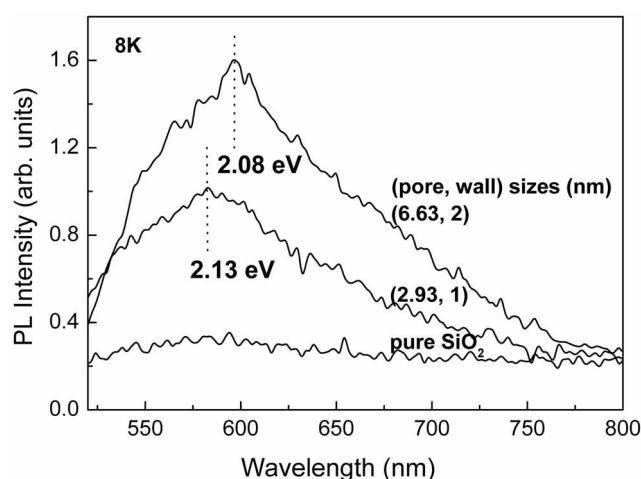


**Figure 6.** PL spectra of calcined mesoporous silica films with different pore and wall sizes together with similar spectrum of pure  $\text{SiO}_2$  without mesopores.

connectivity in this sample than the mesoporous silica films prepared using surfactant templates F 68 and CTACI. The PL spectra were found in the mesoporous silica films prepared using surfactant templates F 68 and CTACI. The mesoporous silica films of 6.63 nm pore size and 3 nm wall thickness show PL spectra at 2.08 eV, which are blue-shifted to 2.13 eV in the samples of smaller pore (2.93 nm) and thinner wall (1 nm). This blue-shift is consistent with that expected from recombination of quantum-confined excitons within nano-sized silica walls.<sup>6</sup> However, the energy of the PL peaks is very smaller than the band gap of silica,  $\sim 11$  eV and consequently, the observed blue-shift cannot be simply attributed to the quantum confinement effect. In Si nano-scale materials, there is some evidence that such blue-shift can originate from the oxygen-related interface states between Si nanocrystals and a surrounding oxide layer.<sup>17,18</sup> It is believed that the defect centers such as nonbridging oxygens should be involved in the optical transitions for the PL shift in this study. No PL peak shifts were found for similar samples by changing their film thickness. These results are in contrast to the previous report<sup>6</sup> that the blue-shift is bigger in larger pore sized materials whose wall is thinner than that of smaller pore sized ones.

## Conclusion

We have shown that mesoporous silica films with different pore sizes have been synthesized by sol-gel spin-coating on Si wafer using TMOS and F 68, Brij 56, or CTACI as the silica source and template, respectively. These materials have optically transparent mesoporous silica films and crack free when thickness is less than 1  $\mu\text{m}$ . The PL properties of these samples strongly depended on their pore size and wall thickness and were interpreted as quantum confinement effect involving defect centers within the nano-sized walls of the silica pores. Mesoporous silica films with different pore sizes contain properties that are more effective in the development of applications for optoelectronic devices.

**Acknowledgments.** J. Y. Bae acknowledges partial support from Keimyung University Foundation Grant (2006). S.-H. Choi acknowledges partial support from the Korea Research Foundation Grant (KRF-2005-005-J00802). This research has been supported by the Korea Science and Engineering Foundation (KOSEF; Grant No. R01-2003-000-10125-0) and the Brain Korea 21 project.

### References

1. Kresge, C. T.; Leonowicz, M. E.; Roth, W. J.; Vartuli, J. C.; Beck, J. S. *Nature* **1992**, *359*, 710.
2. Zhao, D.; Yang, P.; Stucky, G. D. *Adv. Mater.* **1998**, *10*, 1380.
3. Ogawa, M. *Chem. Commun.* **1996**, 1149.
4. Baskaran, S.; Liu, J.; Domansky, K.; Kohler, N.; Li, X.; Coyle, C.; Fryxell, G. E.; Thevuthasan, S.; Williford, R. E. *Adv. Mater.* **2000**, *12*, 291.
5. Doshi, D. A.; Huesing, N. K.; Lu, M.; Fan, H.; Lu, Y.; Simmons-Potter, K.; Potter, Jr. B. G.; Hurd, A. J.; Brinker, J. *Science* **2000**, *290*, 107.
6. Glinka, Y. D.; Lin, S. H.; Hwang, L. P.; Chen, Y. T.; Tolc, N. H. *Phys. Rev. B* **2001**, *64*, 085421-1.
7. Glinka, Y. D.; Lin, S. H.; Hwang, L. P.; Chen, Y. T. *Appl. Phys. Lett.* **2000**, *77*, 3968.
8. Zyubin, A. S.; Glinka, Y. D.; Mebel, A. M.; Lin, S. H.; Hwang, L. P.; Chen, Y. T. *J. Appl. Phys.* **2002**, *116*, 281.
9. Ogawa, M.; Masukawa, N. *Micropor. Mesopor. Mater.* **2000**, *38*, 35.
10. Bae, J. Y.; Jung, J.-I.; Park, O.-H.; Bae, B.-S.; Ranjit, K. T.; Kevan, L. *Stud. Surf. Sci. Catal.* **2003**, *146*, 65.
11. Park, O.-H.; Seo, S.-Y.; Jung, J.-I.; Bae, J. Y.; Bae, B.-S. *J. Mater. Res.* **2003**, *18*(5), 1039.
12. Bertoluzza, A.; Fagnano, C.; Morelli, M. A.; Gottardi, V.; Guglielmi, M. *J. Non-Cryst. Solids* **1982**, *48*, 117.
13. Oliver, S.; Kuperman, A.; Coombs, N.; Louth, A.; Ozin, G. A. *Nature* **1995**, *378*, 47.
14. Bae, J. Y.; Ranjit, K. T.; Luan, Z.; Krishna, R. M.; Kevan, L. *J. Phys. Chem. B* **2000**, *104*, 9661.
15. Luan, Z.; Bae, J. Y.; Kevan, L. *Chem. Mater.* **2000**, *12*, 3202.
16. Bae, J. Y.; Kevan, L. *Micropor. Mesopor. Mater.* **2001**, *50*, 1.
17. Lan, A. D.; Liu, B. X.; Bai, X. D. *J. Appl. Phys.* **1997**, *82*, 5144.
18. Song, H. Z.; Bao, X. M.; Li, N. S.; Wu, X. L. *Appl. Phys. Lett.* **1998**, *72*, 356.